

Numerical Investigation for Enhancement of Heat Transfer in Internally Finned Tubes Using ANSYS CFX Program

Ali Shakir^a

*Al-Furat Al-Awsat^a
Technical University,^b
Department of Mechanical Engineering
University of Basrah
College of Engineering*

Ammar O^b

*Al-Furat Al-Awsat^a
Technical University,^b
Department of Mechanical Engineering
University of Basrah
College of Engineering*

Nofil Baqer^b

*Al-Furat Al-Awsat^a
Technical University,^b
Department of Mechanical Engineering
University of Basrah
College of Engineering*

Abstract- In this study, a numerical investigation has been carried out for single phase flow behavior for thirty six internally finned tubes to demonstrate the effect of axial pitch to fin height ratio (p/e) for $0.8 \leq p/e \leq 6.345$, helix angle of internal fins (β) for $30^\circ \leq \beta \leq 70^\circ$, apex angle of internal fins (α) for $0^\circ \leq \alpha \leq 53.13^\circ$, internal fin height (e) for $0.6 \text{ mm} \leq e \leq 1.0 \text{ mm}$, internal tube diameter (d_i) with 14 mm and Reynolds number (Re) of single phase flow for $10000 \leq Re \leq 50000$ on enhancement of forced convection heat transfer and reduction of friction factor by using ANSYS CFX program. It solves the three-dimensional Navier-Stokes equations for steady state turbulent with SST model and enhance wall treatment. The numerical analysis provided at fully developed velocity and temperature. Numerical results showed that the smallest axial pitch to fin height ratio (p/e) = 0.8 and with apex angle $\alpha = 10$ degree provided enhancement of heat transfer of 2.8 to 3.55 times higher than of smooth tube. Finally, present numerical results are seen to be in good agreement with literature experimental correlations.

Key wards: Internally finned tubes, Turbulent flow model, helix angle, apex angle and fin height

I. Introduction:

Single-phase liquid flow in internally enhanced tubes is becoming more important in commercial HVAC applications, where enhanced tube bundles are used in flooded evaporators and shell-side condensers to increase heat transfer. This enables water chillers to reach high efficiency, which helps mitigate global warming concerns of HVAC systems. One kind of internally enhanced tube is the micro-fin tube.

For experimental study of heat transfer and friction factor, Jacqueline et al. (2004), showed that the heat transfer and friction characteristics for water single-phase flow in micro-fin tubes. They carried the analysis of thermal and hydraulic behavior from a laminar to a turbulent flow out in an experimental setup with a 9.52 mm diameter micro-fin tube. Longjian et al. (2005), performed experimental work to investigate the single-phase flow and flow-boiling heat transfer augmentation in 3D internally finned and micro-finned helical tubes. They carried out the tests for single-phase flow heat transfer augmentation in helical tubes with a curvature of 0.0663 and a length of 1.15 m, and the examined range of the Reynolds number varied from 1000 to 8500. Rahman et al. (2008) presented an experimental investigation of heat transfer enhancement through inner grooved copper tubes in a heat exchanger. They conducted a series of tests to determine the evaporation and condensation performance of the inner grooved copper

tubes namely B3-42 and B16-46 where R-22 was used as the working fluid. Choi, et al. (1999), presented a pressure drop correlation for evaporation and condensation in smooth and micro-fin tubes. The correlation was developed from a database consisting of the following pure and mixed refrigerants: R125, R134a, R32, R410A (R32/R125 50/50 % mass), R22, R407C (R32/R125/R134a, 23/25/52 % mass) and R32/R134a (25/75 % mass). The correlation predicted the measured micro-fin data with an average residual of 10.8 %, and it also predicted the pressure drop in smooth tube with an average residual of 15.0 %. Tam et al. (2010) measured the heat transfer coefficient and pressure drop simultaneously in a single test section and they compared results with the data of a plain tube. From their results, the transition from laminar to turbulent was clearly established and the transition from laminar to turbulent was found to be inlet dependent. Afshin et. al. (2011) measured simultaneously the heat transfer and pressure drop in a single test section fitted with 2 micro-fin tubes and compared with the data of a plain tube. From their results, the transition from laminar to turbulent was clearly established. Wen-Tao et al. (2012) measured turbulent heat transfer and friction factors for 16 internally grooved tubes with different geometrical parameters. Their experiments are conducted for the 16 tubes with the Reynolds number range from 10,000 to 100,000 and Prandtl number from 4.98 to 8.22. Other parameter ranges are: $1 \leq Ns \leq 45$, $0.016 \leq e/d_i \leq 0.04$, $13 \leq a \leq 45$. Guan-Qiu Li et al. (2012) performed an experimental investigation for single-phase flow and condensation characteristics inside five micro-fin tubes with the same outer diameter 5 mm and helix angle 18° . Data for mass fluxes ranging from about 200 to 650 $\text{kg/m}^2 \text{ s}$. Zan Wu et al. (2013) performed an experimental investigation for convective vaporization of R22 and R410A inside one smooth tube and five micro-fin tubes with the same outer diameter of 5 mm. their results suggested that the tube with fin height of 0.15 mm, apex angle of 25° and 38° starts has the best thermal performance for convective vaporization when mass velocity is less than $400 \text{ kg/m}^2 \text{ s}$, while the tube with fin height of 0.12 mm, apex angle of 25° and 58° starts has the best heat transfer performance at larger mass velocities, which is probably due to the relative size between fin height and liquid film thickness.

For numerical study of heat transfer and friction factor, Benzenine et al. (2010) conducted a numerical study for turbulent air flow in the presence of transverse baffles. Two different types of baffles flat rectangular and trapezoidal, arranged in overlapping in a pipe of rectangular section was

presented in their study. Javier Muñoz and Alberto Abánades (2011) analyzed the effect of the utilization of internal finned tubes for the design of parabolic trough collectors with computational fluid dynamics tools. The numerical approach had been qualified with the computational estimation of reported experimental data regarding phenomena involved in finned tube applications and solar irradiation of parabolic trough collector. Piotr (2012) presented theoretical basis and geometry formulation for considering cases and results of numerical simulations for fully developed 3D flow in tubes with micro-fins on the wall. He presented the 3D-chart results in dimensionless and normalized coordinates.

It is very difficult to observe the flow behavior inside internally finned tube using experimental techniques for various axial pitch to fin height ratio, various apex angle and various Reynolds numbers single phase flow on the other hand, numerical technique is a useful technique to investigate the internally flow behavior. In order to explain the flow behavior and heat transfer characteristics inside internally finned tubes a numerical investigation is performed.

Description of the Problem and Geometry

The diameter of each tube is 14 mm and number of fins is 20.while other characteristics are shown in the table 1. The basic algebraic dimensions that define the fin geometry are shown in Fig. 1-a The fin layout parameters are characterized by the fin height (e), pitch normal to the fins (P_f) and the helix angle (β). The number of starts is given by $N_s = \pi d_i \cos \beta / P_f$. The fin shape parameters are defined by the fin base thickness (t), and the apex angle of the fin (α). The axial pitch is defined geometrically by $p_a = \pi d_i / (N_s \tan \beta)$.

The total surface area of the fin tube (A_{actu}) relative to its smooth area (A_s) based on the fin root diameter (d_i), is $A_{actu}/A_s = 1 + 2[\sec(\alpha/2) - \tan(\alpha/2)] * e / P_f$. For a constant tube diameter, a decrease of the fin pitch normal (P_f) will increase the helix angle (β) which provides increased A_{actu}/A_s . and also will increase the apex angle (α) which provides decreased A_{actu}/A_s .

Problem statement and mathematical formulation

The geometry of the problem is presented on Fig. 1-a which shows the characteristic dimensions of grooves details geometry, presented in this work. The system consists of water flow moving through an internally finned tube. The flow is assumed to be turbulent. In this numerical investigation, the following assumptions are adopted (Nofil et al. (2014)):

- I. Physical properties of water are function of temperature.
- II. A profile of velocity is uniform at the inlet.
- III. Radiation heat transfer is negligible.
- IV. Flow inside internally finned tube is assumed to be incompressible steady state turbulent fully developed and the model of SST (Shear Stress Transport) is used.

The 3-D form of the governing equations is maintained since the multi programs in CFD used in the present work is designed to solve 3-D flows past complex geometries, using velocity components and a structured collocated grid.

The governing equations for the flow and heat transfer are that of continuity, Navier–Stokes and the thermal energy as written below (Nofil et al. (2014)):

continuity equation:

$$\frac{\partial}{\partial x}(\rho V_x) + \frac{\partial}{\partial y}(\rho V_y) + \frac{\partial}{\partial z}(\rho V_z) = 0 \dots \dots \dots (1)$$

Momentum equation:

$$\begin{aligned} \frac{\partial}{\partial x}(\rho V_x V_x) + \frac{\partial}{\partial y}(\rho V_y V_x) + \frac{\partial}{\partial z}(\rho V_z V_x) &= \rho g_x - \frac{\partial P}{\partial x} + \frac{\partial}{\partial x} \left(\mu_e \frac{\partial V_x}{\partial x} \right) \\ &+ \frac{\partial}{\partial y} \left(\mu_e \frac{\partial V_x}{\partial y} \right) + \frac{\partial}{\partial z} \left(\mu_e \frac{\partial V_x}{\partial z} \right) + T_x \\ \frac{\partial}{\partial x}(\rho V_x V_y) + \frac{\partial}{\partial y}(\rho V_y V_y) + \frac{\partial}{\partial z}(\rho V_z V_y) &= \rho g_y - \frac{\partial P}{\partial y} + \frac{\partial}{\partial x} \left(\mu_e \frac{\partial V_y}{\partial x} \right) \\ &+ \frac{\partial}{\partial y} \left(\mu_e \frac{\partial V_y}{\partial y} \right) + \frac{\partial}{\partial z} \left(\mu_e \frac{\partial V_y}{\partial z} \right) + T_y \\ \frac{\partial}{\partial x}(\rho V_x V_z) + \frac{\partial}{\partial y}(\rho V_y V_z) + \frac{\partial}{\partial z}(\rho V_z V_z) &= \rho g_z - \frac{\partial P}{\partial z} + \frac{\partial}{\partial x} \left(\mu_e \frac{\partial V_z}{\partial x} \right) \\ &+ \frac{\partial}{\partial y} \left(\mu_e \frac{\partial V_z}{\partial y} \right) + \frac{\partial}{\partial z} \left(\mu_e \frac{\partial V_z}{\partial z} \right) + T_z \end{aligned}$$

Energy equation:

$$\begin{aligned} \frac{\partial}{\partial x}(\rho V_x C_p T) + \frac{\partial}{\partial y}(\rho V_y C_p T) + \frac{\partial}{\partial z}(\rho V_z C_p T) &= \frac{\partial}{\partial x} \left(K \frac{\partial T}{\partial x} \right) + \frac{\partial}{\partial y} \left(K \frac{\partial T}{\partial y} \right) \\ &+ \frac{\partial}{\partial z} \left(K \frac{\partial T}{\partial z} \right) \dots \dots \dots (3) \end{aligned}$$

Where

x, y, z = global Cartesian coordinates,
 V_x, V_y and V_z = components of the vector turbulent velocity in the x, y and z directions, respectively,

$$V_x = \bar{V}_x + \hat{V}_x, \quad V_y = \bar{V}_y + \hat{V}_y, \quad V_z = \bar{V}_z + \hat{V}_z \dots \dots \dots (4)$$

$\bar{V}_x, \bar{V}_y, \bar{V}_z$ = mean components of velocity in x, y and z directions, respectively,

$\hat{V}_x, \hat{V}_y, \hat{V}_z$ = fluctuating components of velocity in x, y and z directions, respectively,

ρ = fluid density,

g_x, g_y, g_z = components of acceleration due to gravity,

μ_e = effective turbulent viscosity = $\mu + \mu_t$ = summation of laminar and turbulent (SST turbulent model) viscosity,

T_x, T_y, T_z = turbulent viscous dissipation term ((Nofil et al. (2014))

The fluid flow was evoked by pressure gradient in a flow direction. The heat flux on inside wall of tube, calculating per unit length, always was set the same $q' = 3000$ W/m, despite of fact, that area of heat transfer between solid wall and fluid was different for every helix angle (Piotr (2012)). In any cases was set the average inlet temperature of fluid equals 305 K (for mentioned temperature of water the Prandtl number is equal about 4.5).

The turbulent model used in the present study is SST. The SST turbulence model combines advantages of both the standard k- ϵ model and the k- ω model. As compared to the turbulence equations in the k- ω model, the SST model first modifies the turbulence production term in the turbulent kinetic energy equation (Nofil et al. (2014)).

Eqs. (1)–(3) have been solved here numerically using CFD program as along with above boundary conditions yields

the velocity, pressure and temperature fields which, in turn, are used to obtain the pressure coefficient, individual and total drag coefficients, and Nusselt number as defined here;

$$\text{Drag coefficient, } C_D = \frac{2 F_D}{\rho U^2 A_p} = C_{Df} + C_{Dp} \dots \dots \dots (5)$$

Where C_{Df} and C_{Dp} are viscous drag and pressure coefficients respectively. and,

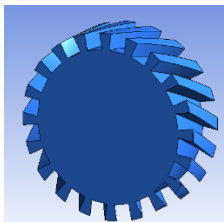
$$\text{Nusselt number, } Nu = \frac{hd_h}{k} \dots \dots \dots (6)$$

Where heat transfer coefficient h (for one axial pitch, Fig 1-a) is calculated in CFX Post program from function calculator, area function, and in at location of fully developed turbulent flow volume region for one axial pitch.

$$\text{Reynolds number, } Re = \frac{\rho V_i d_h}{\mu} \dots \dots \dots (7)$$

Where V_i is the inlet flow velocity (Rahman et a. (2008)).

$$\text{Prandtl number, } Pr = \frac{\mu Cp}{K} \dots \dots \dots (8)$$



One axial pitch volume section

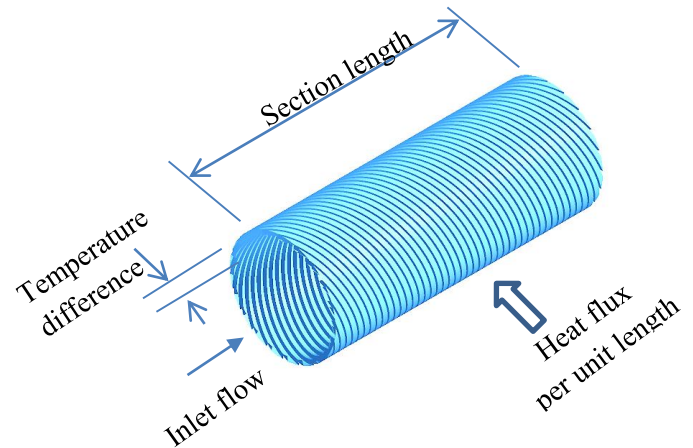
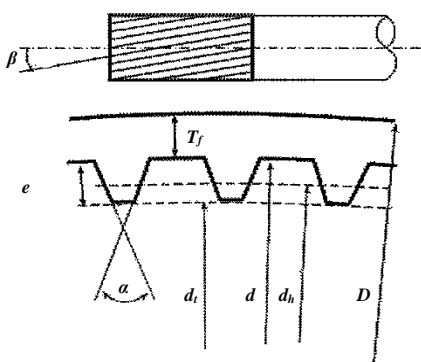
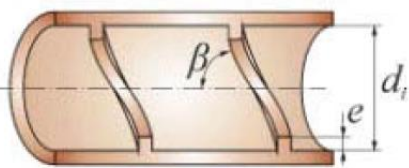


Fig. 1-a Geometrical characterization of micro-fin tubes used to analysis.

Numerical solution methodology:

The first step for any case is to create the project in ANSYS 14.0 / fluid flow (CFX) /Workbench and the study project in (Fig. 1-a) in three dimensional. In ANSYS 14.0 Workbench, the geometry handling tools can be accessed from the Geometry cell on the Project Schematic. You can either create the geometry from scratch in the Design Modeler application or use an existing geometry created in an external CAD package supported by ANSYS 14.0 Workbench. The next step after creating the geometry is to generate a mesh using ICEM CFD to make the mesh generation with high quality. In ICEM CFD program the volume mesh type is Tetra/Mixed with mesh method Robust (Octree). The meshing project is exported to fluid flow (CFX). ANSYS 14.0 was used to calculate the fluid flow throughout the geometry using the computational mesh, and CFD-Post was used to analyze the results. The accuracy and reliability of the numerical results is ascertained by benchmarking them against the available literature values for a few limiting cases.

The conditions of fully developed velocity and temperature profiles have been applied – for all simulations. Special geometrical model (first internally finned tube section without any periodic) has been used as a computational domain. Geometries of one axial section with set of internally-fin were created, which have two ends (inlet and outlet) twisted three turns of 360 degrees. The length of domain was determined by helical angle β . This way of simulation assumes the conditions of translational periodicity on inlet and outlet of the domain (fig. 1-b).

The assumption of periodicity implies that the velocity components repeat themselves in space as follows:

Where

$$u(Z^{\rightarrow}) = u(Z^{\rightarrow} + L^{\rightarrow}) = u(Z^{\rightarrow} + 2L^{\rightarrow}) = \dots \dots \dots (9)$$

$$v(Z^{\rightarrow}) = v(Z^{\rightarrow} + L^{\rightarrow}) = v(Z^{\rightarrow} + 2L^{\rightarrow}) = \dots \dots \dots (10)$$

$$w(Z^{\rightarrow}) = w(Z^{\rightarrow} + L^{\rightarrow}) = w(Z^{\rightarrow} + 2L^{\rightarrow}) = \dots \dots \dots (11)$$

is the position vector and

L is the periodic length vector of the domain considered.

For viscous flows the pressure is not periodic in the sense of equations

$$\Delta p = p(Z^{\rightarrow}) - p(Z^{\rightarrow} + L^{\rightarrow}) = p(Z^{\rightarrow})p(Z^{\rightarrow} + 2L^{\rightarrow}) \dots (12)$$

Instead, the pressure drop between the modules is periodic Since the segregated solver was used the local pressure gradient can be decomposed into two parts: the gradient of a periodic component

$\nabla p \sim (Z \rightarrow)$, and the gradient of a linearly-varying component, $\beta \circ \frac{L \rightarrow}{|L \rightarrow|}$:
 $\nabla p (Z \rightarrow) = \beta \circ \frac{L \rightarrow}{|L \rightarrow|} + \nabla p \sim (Z \rightarrow)$

where $\nabla p \sim (Z \rightarrow)$ is the periodic pressure and $\beta \circ (Z \rightarrow)$ is the linearly-varying component of the pressure. The periodic pressure is the pressure left over after subtracting out the linearly-varying pressure. The linearly-varying component of the pressure results in a force acting on the fluid in the momentum equations. Because the value of β is not known a priori it must be found iteratively until the mass flow rate that has been defined is achieved in the computational model. This correction of β occurs in the pressure correction step of the SIMPLE algorithm, where the value of β is updated based on the difference between the desired mass flow rate and the actual one. The number of substations used to update β is decided by the user.

II. Results and discussions

Distribution of flow temperature

Magnitude of temperature i.e. for Reynolds number equal 10000, fin height 1.0 mm and various helix angle $\beta=30, 50$ and 70 (apex angle $\alpha = 53.13$ / triangular internally fins) at periodic boundary is shown in Fig 2. Because of the effects of increases the secondary flow behavior inside the internally fins due to increase the helix angle (Nofil et al. (2014)), the fluid flow temperature distributions for apex angle $\beta= 70$ is much higher than those in other apex angle and its clearly shown that in fig(2).

Enhancement of heat transfer and friction factor ratio

Dittus-Boelter correlation in eq. 13 for smooth tube is used to predict the heat transfer enhancement over internally finned tubes.

$$Nu_s = \frac{h_s d_i}{k} = 0.023 Re^{0.8} Pr^{0.4} \dots \dots \dots (13)$$

Where h_s is the convection heat transfer coefficient for smooth tube and d_i is the inside diameter of tube.

Figs 3-6 show the variation of enhancement heat transfer for thirty six tubes with various axial pitch to fin height ratio $0.8 \leq p/e \leq 6.345$ and various apex angle $0 \leq \alpha \leq 53.13$. As we can predicted from the present numerical results, the tubes with minimum axial pitch to fin height ratio (maximum helix angle) provided a higher heat transfer enhancement than those for other axial pitch to fin height ratio p/e . It is clearly predicted that the recirculation eddies are growth or created at the internally fin corners. Also, with helix angle increased the intensive and eddies number are increased. Adding that, it is clearly shown that the apex angle $\alpha=10$ degree and axial pitch to fin height ratio $p/e=0.8$ provided 2.8 to 3.55 times higher than those for smooth tube. This is due to the swirling of the flow and it is known to augment heat transfer. Oblique grooves on the internal surface of the tube forcing liquid particles to move spirally. Increased particles speed has the advantage of a significant increase in the amount of heat transfer exchange in spite of increased friction factor or pressure drop (Fig. 7).

Otherwise, Petukhov's friction factor correlation (1970) in equation 14 is used for smooth tubes to provide the friction factor ratio.

$$f_s = (1.58 \ln Re - 3.28)^{-2} \dots \dots \dots (14)$$

Figs 8-11 show the variation of friction factor ratio with Reynolds number between 10000-50000 for various apex

angle for thirty six internally finned tubes. It is clearly shown that lower axial pitch to fin height ratio provided higher friction factor ratio. In spite that internally finned tubes provided higher heat transfer enhancement, the friction factor ratio is provided more times heat transfer enhancement.

III. Validation

After the main calculations, a validation of numerical simulation have been carried out. Comparison between the present numerical values and the correlations for previous workers for enhancement heat transfer and friction factor ratios are clearly shown in Figs 12 and 13.

First correlations were used in the present work are for Ravigururajan and Bergles (1985). They carried out work on internally finned tubes. They predicted the correlation for heat transfer as in the following:

$$\frac{Nu}{Nu_s} = \left\{ 1 + \left[2.64 Re^{0.036} \left(\frac{e}{d}\right)^{0.212} \left(\frac{p_a}{d}\right)^{-0.21} \left(\frac{\alpha}{90}\right)^{0.29} Pr^{-0.024} \right]^7 \right\}^{\frac{1}{7}} \dots (15)$$

Heat transfer correlation in above predicted 99% of their database to within $\pm 50\%$ and 69% to within $\pm 20\%$.

Also, the correlations presented by Webb, Narayanamurth and Thors, (2000) for calculating the heat transfer coefficient and friction factor for internally ribs or finned tubes were used in the comparison of the present numerical data and their correlation as follows;

$$St Pr^{2/3} = 0.00933 Re^{-0.181} N_s^{0.0285} \left(\frac{e}{d}\right)^{0.323} \beta^{0.505} \dots (16)$$

Where N_s is the number of stars, dimensionless.

$$f = 0.108 Re^{-0.283} N_s^{0.212} \left(\frac{e}{d}\right)^{0.785} \beta^{0.78} \dots \dots \dots (17)$$

The comparison between the present numerical results and the correlations for enhancement heat transfer and friction factor ratios are clearly shown in Figs 11 and 12. Present numerical results (i.e. helix angle $\beta=70$ deg., apex angle $\alpha=10$ deg., fin height $e=0.8$ mm. and for variation Reynolds number $20000 \leq Re \leq 50000$) are seen to be in good agreement with above correlations for heat transfer and in a reasonable agreement for friction factor. Such a close correspondence inspires confidence in the reliability of the results obtained in this study for the internally finned tubes.

IV. Conclusions

Designs can be performed for many types of systems with the computer approach outlined. Hopefully, designers will recognize the significant performance improvements possible for many applications with the use of internally finned tubes.

Numerical analysis is performed to investigate the single phase flow and flow-boiling heat transfer augmentation in 3D internally finned and micro-finned helical tubes. The conclusions can be summarized as follows:

1. The higher amount of forced convection heat transfer occurs at a lower axial pitch to fin height ratio $p/e = 0.8$. For closely spaced fins, intensive recirculation eddies are trapped between internal fins and enhanced forced convection heat transfer
2. Friction factor for various axial pitch to fin height ratio p/e is higher for larger helix angle β .

3. Smallest axial pitch to fin height ratio $p/e = 0.8$ and with apex angle $\alpha = 10$ degree provided enhancement of heat transfer of 2.8 to 3.55 times higher than of smooth tube.

V. References

- [1] Jacqueline Biancon Copetti*, Mario Henrique Macagnan, Daiana de Souza, Rejane De Ce'saro Oliveski. , "Experiments with micro-fin tube in single phase". International Journal of Refrigeration, 27, 876–883, 2004.
- [2] Longjian Li, Wenzhi Cui, Quan Liao, Xin Mingdao, Tien-Chien Jen, Qinghua Chen., "Heat transfer augmentation in 3D internally finned and micro finned helical tube". International Journal of Heat and Mass Transfer, 48, 1916–1925, 2005.
- [3] M. M. Rahman, Y. M. Ling, G. W. Soon., "An Experimental Investigation of Condensation and Evaporation Heat Transfer of R-22 inside Internally Grooved Copper Tubes". ICCBT.F. (04) , pp35-48, 2008.
- [4] Choi, J. Y., Kedzierski, M. A., and Domanski, P. A., "Generalized Pressure Drop Correlation for Evaporation and Condensation of Alternative Refrigerants in Smooth and Micro-fin Tubes", NISTIR 6333, 2009.
- [5] H. K. Tam, L. M. Tam, W. W. Chu, A. J. Ghajar., "Experimental analysis of the single-phase heat transfer and friction factor inside the horizontal internally micro-fin tube". 2nd international conference on mechanical and electronics engineering, ICMEE, 2010.
- [6] Afshin J. Ghajar , Lap Mou Tam , Hou Kuan Tam., "Experimental analysis of the single-phase heat transfer and friction factor inside the horizontal internally micro-fin tube". Thermal engineering joint conference, 2011, Honolulu, Hawaii, USA AJTEC, 2011-4455, 2011.
- [7] Wen-Tao Ji, Ding-Cai Zhang, Ya-Ling He, Wen-Quan Tao., "Prediction of fully developed turbulent heat transfer of internal helically ribbed tubes An extension of Gnielinski equation". International Journal of Heat and Mass Transfer, 55, 1375–1384, 2012..
- [8] Guan-Qiu Li , Zan Wu, Wei Li , Zhi-Ke Wang , Xu Wang, Hong-Xia Li , Shi-Chune Yao., "Experimental investigation of condensation in micro-fin tubes of different geometries". Experimental thermal and fluid science, 37, 19–28, 2012.
- [9] Zan Wua, Yang Wuc, Bengt Sundén, Wei Li., "Convective vaporization in micro-fin tubes of different geometries". Experimental Thermal and Fluid Science, 44, 398–408, 2013.
- [10] H. Benzenine, R. Saim, S. Abboudi, O. Imine., "Numerical simulation of the dynamic turbulent flow field through a channel provided with baffles" Comparative study between two models of baffles: transverse plane and trapezoidal. Revue des Energies Renouvelables Vol. 13, No.4 639 – 651, 2010.
- [11] Javier Muñoz , Alberto Abánades., "Analysis of internal helically finned tubes for parabolic trough design by CFD tools", Universidad Politécnica de Madrid, J.Gutiérrez Abascal, 2, 28006 Madrid, Spain, 2011.
- [12] Piotr Jasinski., "Numerical optimization of flow-heat ducts with helical micro-fins, using Entropy Generation Minimization (EGM) method", Recent Advances in Fluid Mechanics and Heat & Mass Transfer Department of Heat Technology and Refrigeration Technical, University of Iodź ul, Stefanowskiego 1/15, 90-924 ,2012.
- [13] Nofil Baqer, Ali Shakir and Ammar O., "Computational Investigation of Enhancement Heat Transfer of 3D Internally Finned Tubes Using Ansys CFX" M.Sc. Thesis, University of Basrah, Engineering College, Mechanical Engineering, 2014.
- [14] Petukhov, B.S., "Heat Transfer and Friction in Turbulent Pipe Flow with Variable Physical Properties"., Advances in Heat Transfer, Academic Press, New York, Vol. 6, pp. 503-564, 1970.
- [15] Ravigururajan, T.S. and Bergles, A.E., "General Correlations for Pressure Drop and Heat Transfer for Single-Phase Turbulent Flow in Internally Ribbed Tubes", Augmentation of Heat Transfer in Energy Systems, ASME HTD Vol. 52, pp. 9-20, 1985.
- [16] R.L. Webb, N.H. Kim, Principle of Enhanced Heat Transfer, second ed., Taylor & Francis, Boca Raton, 2005.

VI. Symbols

Symbols	Description	Units
C_p	Specific heat capacity	J/ (Kg.C)
D	Outside diameter	m
d	Root diameter	
d_i	Internal diameter of tube	m
d_h	Hydraulic diameter of tube	m
e	Fin height	m
f	Friction factor	
f_s	Friction factor for smooth tube	
h	Heat transfer coefficient for one axial pitch volume section	W/m ² .K
h_{pt}	Heat transfer coefficient on plane tube	W/m ² .K
L	Length	m
k	Thermal conductivity	W/m.K
N_s	Numbers of stars	
Nu	Nusselt number	
P	Pressure	KPa
P	Fin axial pitch	mm
Pr	Prandtl number of liquid	
Pr_s	Prandtl number of liquid for smooth tube	
Nu	average Nusselt number	
Nus	Average Nusselt number for smooth tube	
q	wall heat flux per unit length	W/m
Re	Reynolds number	
St	Stanton number	
T_f	Thickness of tube	m
n	Number of grooves	

VII. Creek Symbol

α	Apex angle	Deg
β	Helices angle	Deg
ρ	Density	kg/m ³
μ	molecular (dynamic) viscosity	kg/(m s)

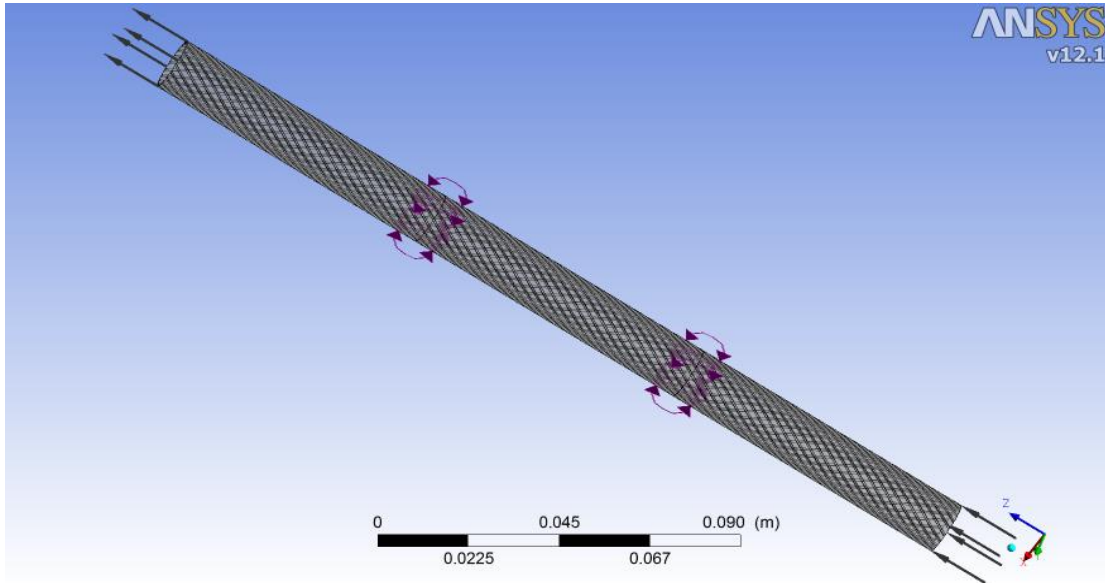
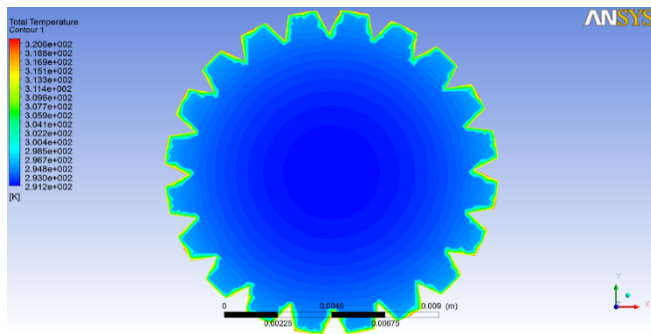
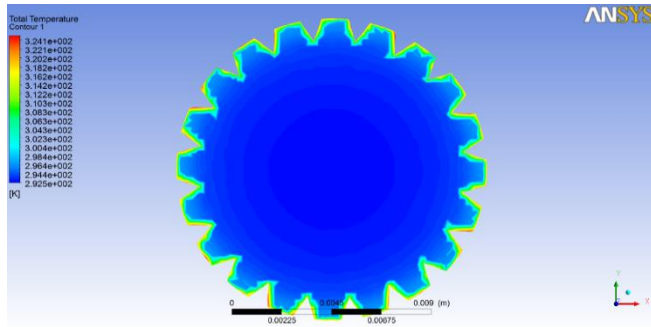


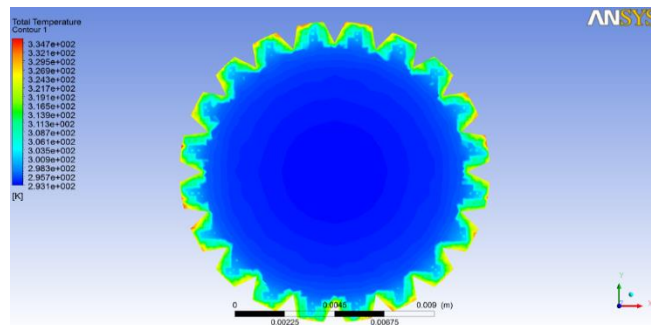
Fig. 1-b Periodic flow techniques.



$\beta=30$ deg.
Re=10000
Fin height = 10 mm
 $\alpha=53.13$



$\beta=50$ deg.
Re=10000
Fin height = 10 mm
 $\alpha=53.13$



$\beta=70$ deg.
Re=10000
Fin height = 10 mm
 $\alpha=53.13$

Fig. 2 flow temperature distributions along internally finned tubes with various parameters.

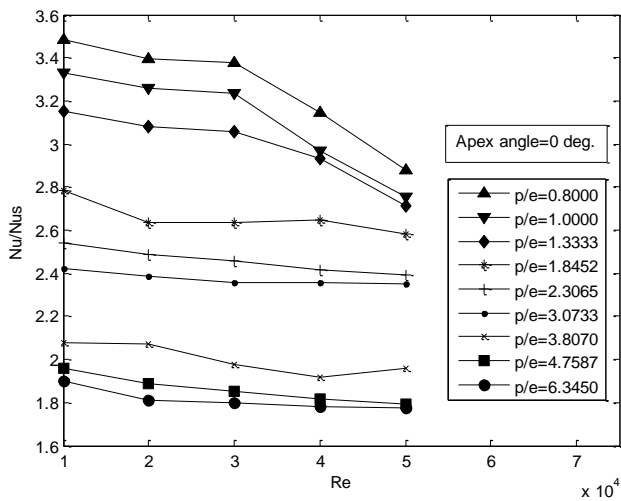


Fig. 3 Enhancement heat transfer vs. Reynolds number at various p/e ratio and at apex angle $\alpha=0$ deg.

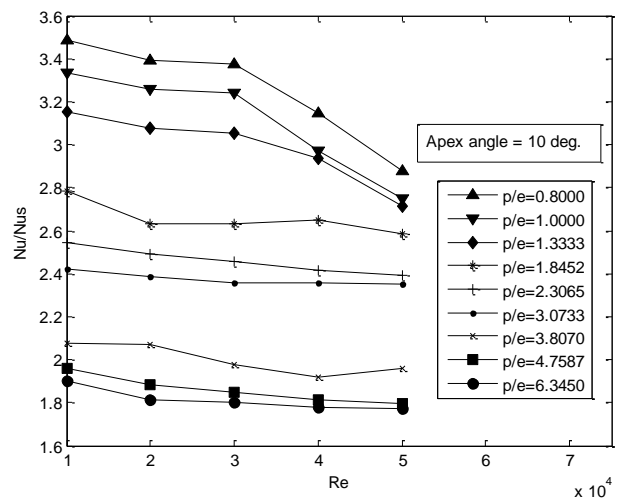


Fig. 4 Enhancement heat transfer vs. Reynolds number at various p/e ratio and at apex angle $\alpha=10$ deg.

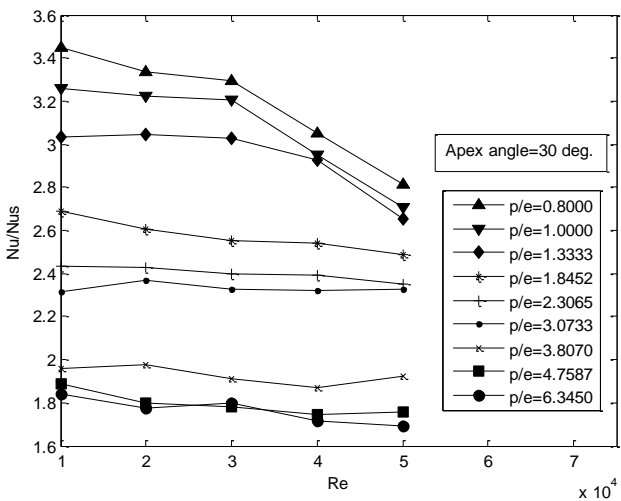


Fig. 5 Enhancement heat transfer vs. Reynolds number at various p/e ratio and at apex angle $\alpha=30$ deg.

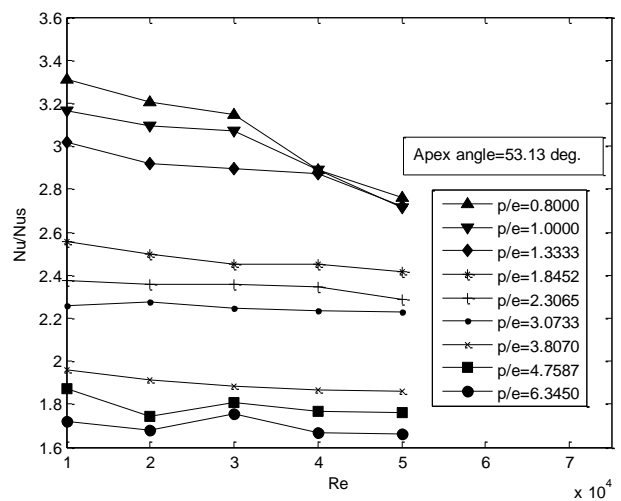


Fig. 6 Enhancement heat transfer vs. Reynolds number at various p/e ratio and at apex angle $\alpha=53.13$ deg.

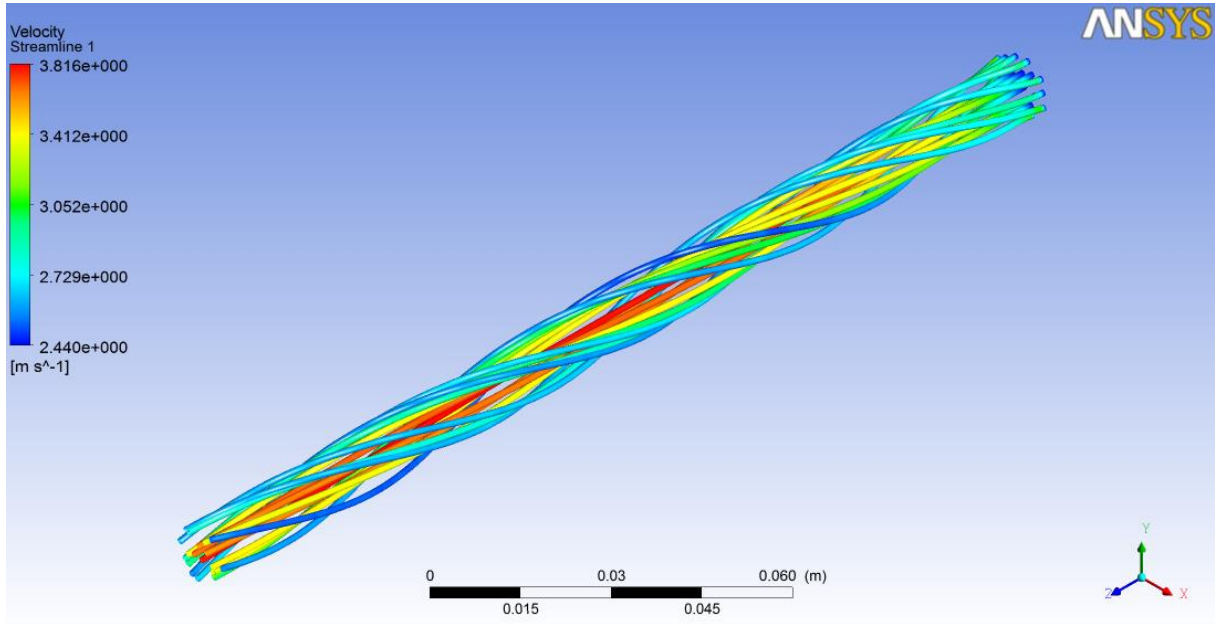


Fig. 7 Fluid particles velocity shape in a fully turbulent flow region and the velocity streamlines for the flow at $Re=30000$, $\beta=70$ deg., $\alpha=0$ deg., $e=1$ mm.

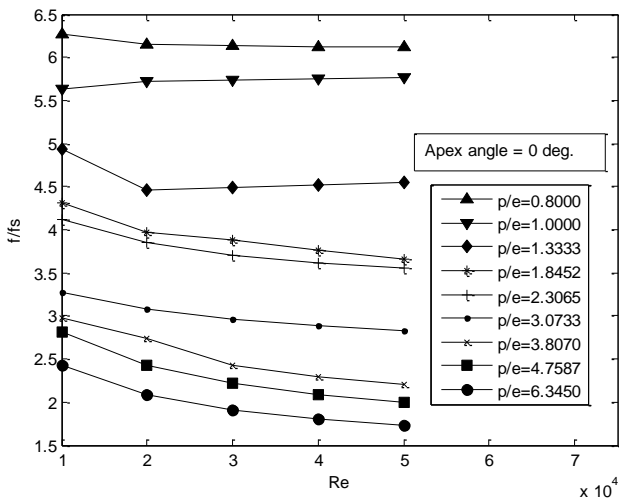


Fig. 8 Friction factor ratio vs. Reynolds number at various p/e ratio and at apex angle $\alpha=0$ deg.

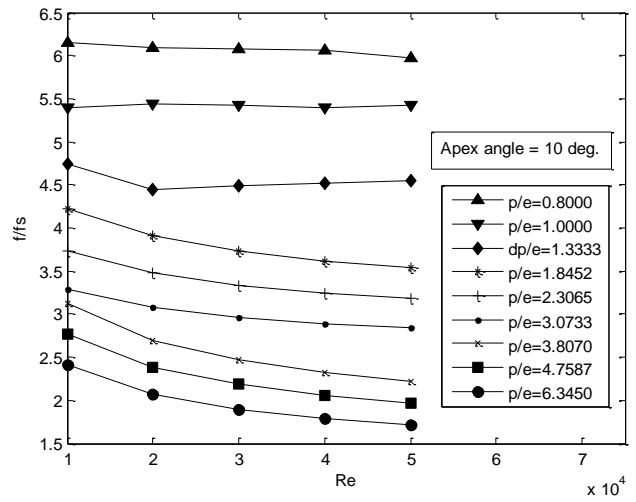


Fig. 9 Friction factor ratio vs. Reynolds number at various p/e ratio and at apex angle $\alpha=10$ deg.

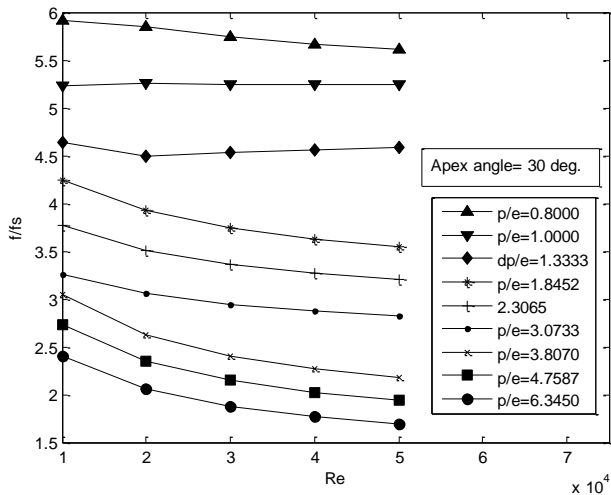


Fig. 10 Friction factor ratio vs. Reynolds number at various p/e ratio and at apex angle $\alpha=30$ deg.

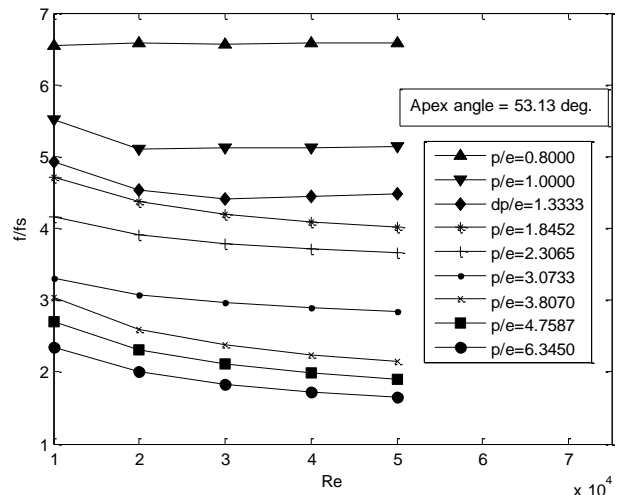


Fig. 11 Friction factor ratio vs. Reynolds number at various p/e ratio and at apex angle $\alpha=53.13$ deg.

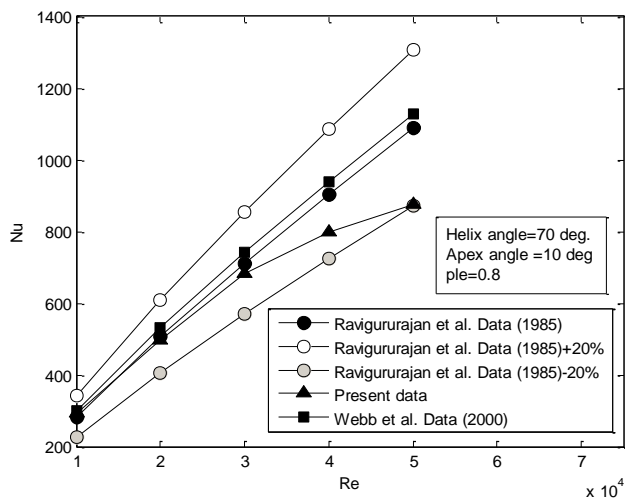


Fig. 12 comparison of present numerical results with previous workers at helix angle $\beta=70$ deg., apex angle $\alpha=10$ deg., fin height $e=0.8$ mm

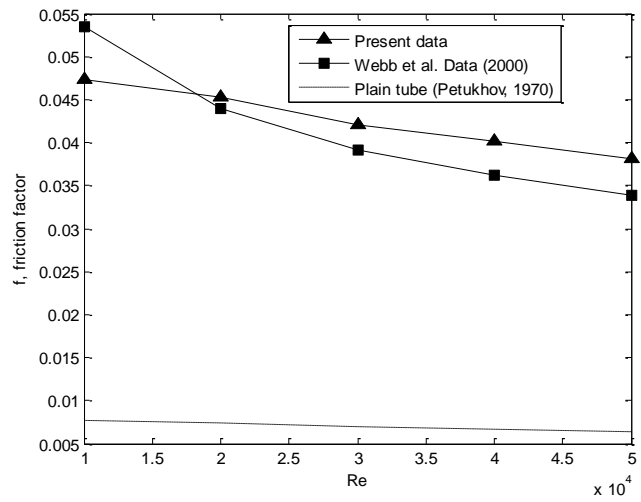


Fig. 13 comparison of present numerical results with previous workers at helix angle $\beta=70$ deg., apex angle $\alpha=10$ deg., fin height $e=0.8$ mm.

Table I Dimensions of the geometries.

Tube model	d_i (mm)	β (deg)	α (deg)	e(mm)	P_a (mm)	P_f (mm)	A_{acti}/A_s
1	14	30	0	1	3.807	1.905	2.0499
2	14	30	10	1	3.807	1.905	1.9621
3	14	30	30	1	3.807	1.905	1.8058
4	14	30	53.13	1	3.807	1.905	1.6562
5	14	50	0	1	1.8452	1.414	2.4141
6	14	50	10	1	1.8452	1.414	2.2958
7	14	50	30	1	1.8452	1.414	2.0852
8	14	50	53.13	1	1.8452	1.414	1.8838
9	14	70	0	1	0.8	0.753	3.6546
10	14	70	10	1	0.8	0.753	3.4326
11	14	70	30	1	0.8	0.753	3.0372
12	14	70	53.13	1	0.8	0.753	2.6592
13	14	30	0	0.8	3.807	1.905	1.8399
14	14	30	10	0.8	3.807	1.905	1.7697
15	14	30	30	0.8	3.807	1.905	1.6446
16	14	30	53.13	0.8	3.807	1.905	1.5250
17	14	50	0	0.8	1.8452	1.414	2.1313
18	14	50	10	0.8	1.8452	1.414	2.0366
19	14	50	30	0.8	1.8452	1.414	1.8681
20	14	50	53.13	0.8	1.8452	1.414	1.7070
21	14	70	0	0.8	0.8	0.753	3.1237
22	14	70	10	0.8	0.8	0.753	2.9461
23	14	70	30	0.8	0.8	0.753	2.6298
24	14	70	53.13	0.8	0.8	0.753	2.3273
25	14	30	0	0.6	3.807	1.905	1.6299
26	14	30	10	0.6	3.807	1.905	1.5773
27	14	30	30	0.6	3.807	1.905	1.4834
28	14	30	53.13	0.6	3.807	1.905	1.3937
29	14	50	0	0.6	1.8452	1.414	1.8484
30	14	50	10	0.6	1.8452	1.414	1.7775
31	14	50	30	0.6	1.8452	1.414	1.6511
32	14	50	53.13	0.6	1.8452	1.414	1.5303
33	14	70	0	0.6	0.8	0.753	2.5927
34	14	70	10	0.6	0.8	0.753	2.4595
35	14	70	30	0.6	0.8	0.753	2.2223
36	14	70	53.13	0.6	0.8	0.753	1.9955